J Supercond Nov Magn (2014) 27:1603–1614
DOI 10.1007/s10948-014-2540-1

REVIEW PAPER

First-Principle Investigations of Structural, Electronic, and Half-Metallic Ferromagnetic Properties in $In_{1-x}TM_xP$ (TM = Cr, Mn)

M. Boutaleb · A. Tadjer · B. Doumi · A. Djedid · A. Yakoubi · F. Dahmane · B. Abbar

Received: 2 March 2014 / Accepted: 11 March 2014 / Published online: 3 May 2014

Abstract First-principle calculations within the framework of density functional theory are employed to study the structural, electronic, and half-metallic ferromagnetic properties of $In_{1-x}TM_xP$ (TM = Cr, Mn) at concentrations (x = 0.0625, 0.125, 0.25) of transition metal (TM) in zinc blende phase. The investigations of electronic and magnetic properties indicate that $In_{1-x}TM_xP$ (TM = Cr, Mn) at x = 0.0625, 0.125, and 0.25 are half-metallic ferromagnets with 100 % magnetic spin polarization. On the one hand, the total magnetization is an integer Bohr magneton of $3\mu_B$ and $4\mu_B$ for $In_{1-x}Cr_xP$ and $In_{1-x}Mn_xP$, respectively, which confirms the half-metallic feature of $In_{1-x}TM_xP$ compounds. On the other hand, the densities of states of majority-spin states show that the large hybridization between 3p (P) and 3d (TM) partially filled states dominates the gap, which stabilizes the ferromagnetic state configuration associated with double-exchange mechanism. The band structures depict that half-metallic gap at x = 0.0625 is 0.404 eV for $In_{1-x}Cr_xP$ which is higher than 0.125 eV for $In_{1-x}Mn_xP$. Therefore, the largest half-metallic gap in $In_{1-x}Cr_xP$ at low concentration x = 0.0625 reveals that Cr-doped InP seem to be a more potential candidate than that Mn-doped InP for spin injection applications in the field of spintronic devices.

Keywords Spintronics · Half metals · Ferromagnetic properties · Electronic structures · (Cr · Mn)-doped InP

M. Boutaleb (✉) · A. Tadjer · B. Doumi · A. Djedid · A. Yakoubi · F. Dahmane · B. Abbar
Modelling and Simulation in Materials Science Laboratory, Physics Department, Djillali Liabes University of Sidi Bel-Abbes, 22000, Sidi Bel-Abbes, Algeria
e-mail: mbouttaleb@yahoo.fr

1 Introduction

The 3*d* transition metals (TMs) grown on semiconductors have attracted a special interest over the last two decades, owing to the possibility of combining magnetism and semiconductor properties and offering a wide range of possible applications [1]. However, the magnetic property in diluted magnetic semiconductors (DMSs) doped by 3*d* (TM) ions leads to an interaction between the localized spin-polarized *d* electrons of the TM impurities and the delocalized carriers in the host semiconductor [2]. In recent years, the III–V-based DMSs can be considered to be promising materials for a new generation of spin-based electronics or spintronics devices [3–5], because they exhibit two essential features: a Curie temperature (T_C) higher than room temperature and half-metallic ferromagnetic (HMF) properties. Thus, the HMF nature of DMS takes an important role in the newly developing field of spintronics, in particular, as an origin of spin-polarized carriers injected into semiconductors. During the last 2 years, the HMF properties have been investigated in TM-doped III–V and II–VI semiconductors such as $(Ga, Al, In)_{1-x}Mn_xN$ [6, 7], $(Ga, In)_{0.75}Mn_{0.25}P$ [8], Cr-doped GaP [9], $Ga_{1-x}Mn_x(P, As)$ [10], V-doped AlN [11], V-doped GaN [12], (V, Cr, Mn, Fe)-doped GaN [13], Mn-doped BN [14], $Cd_{1-x}Cr_x(S, Se, Te)$ [15], V-doped CdTe [16], $Cd_{1-x}Fe_xS$ [17], $Cd_{1-x}V_xSe$ [18], $Zn_{0.75}Cr_{0.25}(S, Se, Te)$ [19], $Zn_{1-x}Cr_xS$ [20], $Be_{0.75}Mn_{0.25}(S, Se, Te)$ [21], $Be_{1-x}Mn_x(Se, Te)$ [22], Cr-doped BeSe and BeTe [23], and V-doped Be(S, Se, Te) [24].

The InP is a useful compound semiconductor due to its excellent physical properties and good characteristics for application to various devices. It has been found to be attractive for long-wavelength optoelectronics and for high-speed and high-power electronic devices [25]. So, it is used as a substrate for high-speed electrical and optoelectronic

device like high-frequency field effect transistors and resonant interband tunneling diodes [26, 27], although the InP semiconductor is considered as a possible candidate as a DMS material according to a theoretical report [28] and to the experimental results of Hollingsworth et al. [29], which constitute the highest reported T_C (∼130 K) in Mn-doped InP. In addition, Korona et al. [30] shown that the Mn^{+3} center in InP had some features of a well-localized center and some of a weakly localized one, where the Mn is a relatively deep acceptor in III-Mn-V, and its level is 0.22 eV above the valence band maximum in InP [31]. Also, the ferromagnetism has been theoretically reported for magnetic Mn–Mn coupling in the Mn-doped InP nanowires [32], and the robustness of half-metallicity was theoretically predicted in $In_{0.75}Mn_{0.25}P$ [8].

In this present study, we investigate the structural, electronic, and magnetic properties of zinc blende phase $In_{1-x}TM_xP$ (TM = Cr, Mn) at concentrations ($x = 0.0625$, 0.125, 0.25) and to use them to predict the half-metallic ferromagnetism behavior, based on simple ordered supercell of 32, 16, and 8 atoms, using first-principle full-potential linearized augmented plane-wave method (FP-LAPW) with generalized gradient approximation functional proposed by Wu and Cohen (WC-GGA).

2 Method of Calculations

The calculations of the present study are performed in the framework of the density functional theory (DFT) [33, 34]. We have employed the FP-LAPW method as implemented in the WIEN2 k code [35]. The WC-GGA was used for the exchange correlation potential [36] in order to investigate the electronic and half-metallic ferromagnetic properties of (TM = Cr, Mn)-doped InP in zinc blende structure, based on $In_{15}TMP_{16}$, In_7TMP_8, and In_3TMP_4 supercells of 32, 16, and 8 atoms, respectively, where the $In_{1-x}TM_xP$ is obtained by substituting one TM atom in an In cation site.

The InP has zinc blende (B3) structure with space group $F\bar{4}3m$, where the In atom is located at position (0, 0, 0) and P atom at (0.25, 0.25, 0.25). We obtain the $In_{1-x}TM_xP$ compounds at concentrations $x = 0.0625$, $x = 0.125$, and $x = 0.25$ by substituting one In cation with one (TM = Cr, Mn) atom in supercells of 32, 16, and 8 atoms, respectively, to get the $In_{0.9375}TM_{0.0625}P$ ($1 \times 2 \times 2$) supercell of 32 atoms with $x = 0.0625$ of tetragonal structure with space group $P\bar{4}2m$, $In_{0.875}TM_{0.125}P$ ($1 \times 1 \times 2$) supercell of 16 atoms with $x = 0.125$ of tetragonal structure with space group $P\bar{4}2m$, and $In_{0.75}TM_{0.25}P$ ($1 \times 1 \times 1$) standard unit cell of 8 atoms with $x = 0.25$ of cubic structure with space group $P\bar{4}3m$ as shown in Fig. 1.

The non-overlapping muffin–tin radii (R_{MT}) of In, P, Cr, and Mn are taken to be as large as possible in such a way that the spheres do not overlap. We have expanded the wave functions in the interstitial region to plane waves with a cut-off of $K_{max} = 8.0 / R_{MT}$ (where K_{max} is the magnitude of the largest K vector in the plane wave, and R_{MT} is the average radius of the muffin–tin spheres). The maximum value for partial waves inside the atomic sphere was $l_{max} = 10$, while the charge density was Fourier expanded up to $G_{max} = 12$, where G_{max} is the largest vector in the Fourier expansion. For the sampling of the Brillouin zone, $2 \times 2 \times 5$, $4 \times 4 \times 2$, and $4 \times 4 \times 4$ Monkhorst–Pack mesh [37, 38] are utilized for supercells of 32, 16, and 8 atoms, respectively, where the self-consistent convergence of the total energy was at 0.1 mRy.

3 Results and Discussions

3.1 Structural Properties

The structural parameters such as equilibrium lattice constant (a), bulk modulus (B), and its pressure derivative ($B\prime$) for binary zinc blende InP and the $In_{1-x}TM_xP$ compound supercells as a function of the concentration (x) are calculated by fitting of variation of total energies and equilibrium volumes with the empirical Murnaghan's equation of state [39]. Our results and various theoretical [8, 40] and experimental [41, 42] data are given in Table 1.

The ground-state properties a, B, and $B\prime$ for zinc blende InP are very close to the theoretical WC-GGA calculations of Tran et al. [40] and are in good agreement with experimental values [41, 42]. For the ternary $In_{1-x}TM_xP$ (TM = Cr, Mn) at concentrations ($x = 0.0625$, 0.125, 0.25), there are some decrease in the lattice constants with an increasing concentration (x) of (TM = Cr, Mn), which can be attributed to the fact that the ionic radius of Cr and Mn is smaller than that of In atom. The bulk modulus increases when the concentration x of (TM = Cr, Mn) increases, and we notice that the lower bulk modulus of $In_{1-x}Cr_xP$ compounds are easily compressible than that of $In_{1-x}Mn_xP$ higher ones. In addition, we observe an enhancement by −2.95 % of our calculated lattice constant of $In_{0.75}Mn_{0.25}P$ compared with theoretical calculations of Djedid et al. [8] by using the generalized gradient approximation of Perdew et al. [43] (GGA-PBE). To the best of our knowledge, there are no experimental and theoretical WC-GGA calculations of lattice constant, bulk modulus, and its pressure derivative for $In_{1-x}TM_xP$ (TM = Cr, Mn) at concentrations of $x = 0.0625$, 0.125, and 0.25 to compare with the results of our present work.

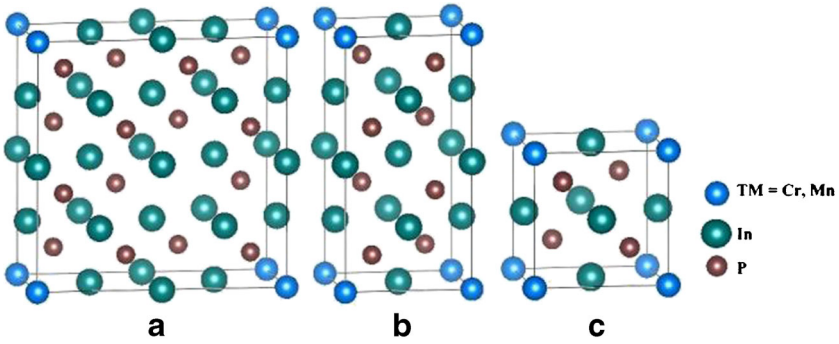

Fig. 1 The prototype structures of $In_{1-x}TM_xP$ compounds with (TM = Cr, Mn). *a* $In_{0.9375}TM_{0.0625}P$ supercell of 32 atoms with $x = 0.0625$, *b* $In_{0.875}TM_{0.125}P$ supercell of 16 atoms with $x = 0.125$, and *c* $In_{0.75}TM_{0.25}P$ standard unit cell of 8 atoms with $x = 0.25$

3.2 Electronic Properties

The electronic structures are discussed in order to describe and investigate the mechanism of formation of the half-metallic ferromagnetic behavior in $In_{1-x}TM_xP$ (TM = Cr, Mn) compounds. The spin-resolved total (*T*) and partial (*P*) density of states (DOS) for $In_{0.9375}Cr_{0.0625}P$, $In_{0.875}Cr_{0.125}P$, $In_{0.75}Cr_{0.25}P$, $In_{0.9375}Mn_{0.0625}P$, $In_{0.875}Mn_{0.125}P$, and $In_{0.75}Mn_{0.25}P$ are shown in Figs. 2, 3, 4, 5, 6, and 7, respectively. According to the crystal field theory [44], it is understandable that the effect of the tetrahedral crystal field formed by surrounding P ligands in $In_{1-x}TM_xP$ splits the 3*d* (TM = Cr, Mn) states into twofold, generating low-lying e_g $\left(d_{z^2}\right.$ and $\left.d_{x^2-y^2}\right)$ and threefold, degenerating high-lying t_{2g} $\left(d_{xy}, d_{xz},\right.$ and $\left.d_{yz}\right)$ symmetry states [45] displayed in PDOS (Figs. 2, 3, 4, 5, 6, and 7). From these plots, we show that the t_{2g} states lie above the e_g states, and this reveals that the energy of e_g states is lower than that of t_{2g} states due to less Coulomb interaction [46]. It means that Cr and Mn are sitting in the crystalline field of tetrahedron. However, the PDOS demonstrates that the top of the majority-spin valence bands and the bottom of the minority-spin conduction bands are dominated by 3*d* (TM = Cr, Mn) states, which hybridize with the 3*p* (P) states. Also, these PDOSs depict that there are strong hybridization between 3*d* (TM = Cr, Mn) and 3*p* (P) states that make the host valence band. This creates bonding states (t^b) in the valence bands and anti-bonding states (t^a) in the band gap, while the e_g states extend to the interstitial region and hybridize very weakly with the host valence states to make non-bonding states (*e*) in the gap [47–49]. It is found that the anti-bonding states principally come from the 3*d*-t_{2g} (TM = Cr, Mn) and 3*p* (P) states.

The curves of densities of states show a half-metallic ferromagnetic behavior of $In_{1-x}TM_xP$ at all concentrations ($x = 0.0625, 0.125, 0.25$) of (TM = Cr, Mn). This may be attributed to the fact that the minority-spin states have a band gap, whereas the majority-spin states have a metallic character. The majority-spin channel of $In_{1-x}TM_xP$ is

Table 1 Calculation of lattice constant (*a*), bulk modulus (*B*), and its pressure derivative (*B′*) for binary InP and $In_{1-x}TM_xP$ at concentrations ($x = 0.0625$, 0.125, 0.25) of (TM = Cr, Mn)

Compound	Concentration (*x*)	a (A^0)	*B* (GPa)	*B′*
This work				
InP	0.00	5.893	66.55	4.86
$In_{1-x}Cr_xP$	0.0625	5.847	68.19	5.00
	0.125	5.811	70.77	4.79
	0.25	5.734	75.99	4.72
$In_{1-x}Mn_xP$	0.0625	5.841	68.72	4.99
	0.125	5.801	70.89	4.91
	0.25	5.714	76.78	5.07
Other calculations				
InP	0.00	5.890 [40]	67.40 [40]	
		5.869 [41]	72.00 [42]	
$In_{1-x}Mn_xP$	0.25	5.888 [8]	61.14 [8]	5.11 [8]

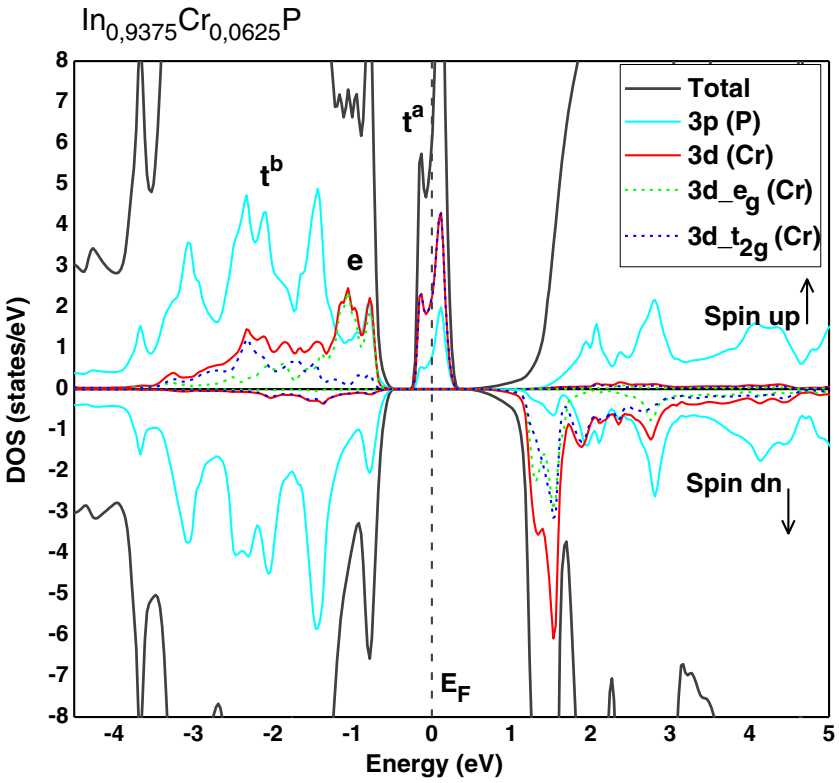

Fig. 2 Spin-polarized total and partial DOS of (3*p*) of P and (3*d*, 3*d*-e_g, 3*d*-t_{2g}) of Cr in supercell for $In_{0.9375}Cr_{0.0625}P$. The Fermi level is set to zero (*dotted line*)

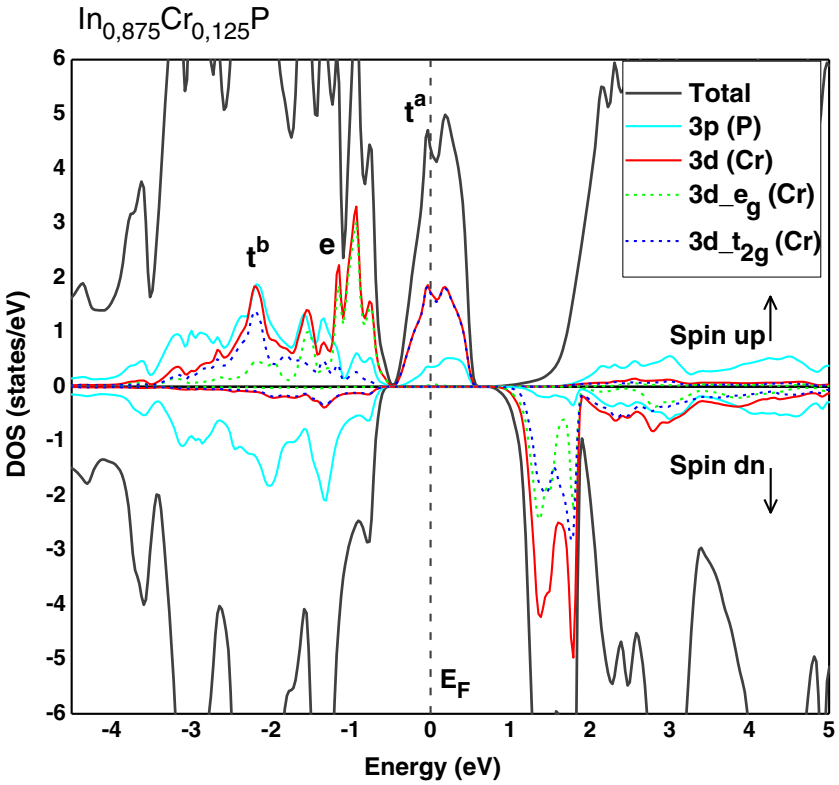

Fig. 3 Spin-polarized total and partial DOS of (3*p*) of P and (3*d*, 3*d*-e_g, 3*d*-t_{2g}) of Cr in supercell for $In_{0.875}Cr_{0.125}P$. The Fermi level is set to zero (*dotted line*)

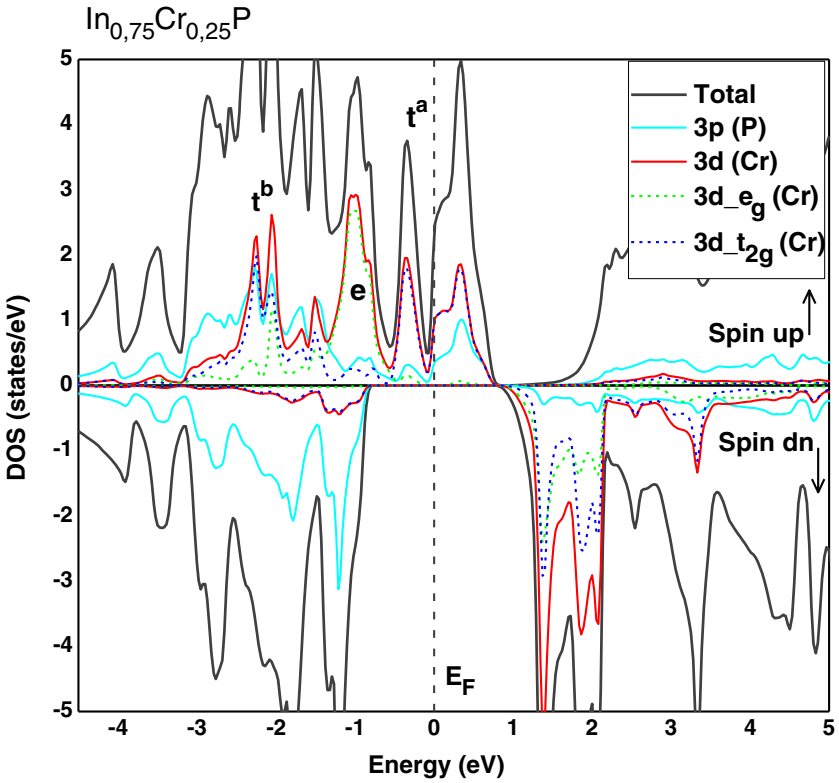

Fig. 4 Spin-polarized total and partial DOS of (3*p*) of P and (3*d*, 3*d*-e_g, 3*d*-t_{2g}) of Cr in supercell for $In_{0.75}Cr_{0.25}P$. The Fermi level is set to zero (*dotted line*)

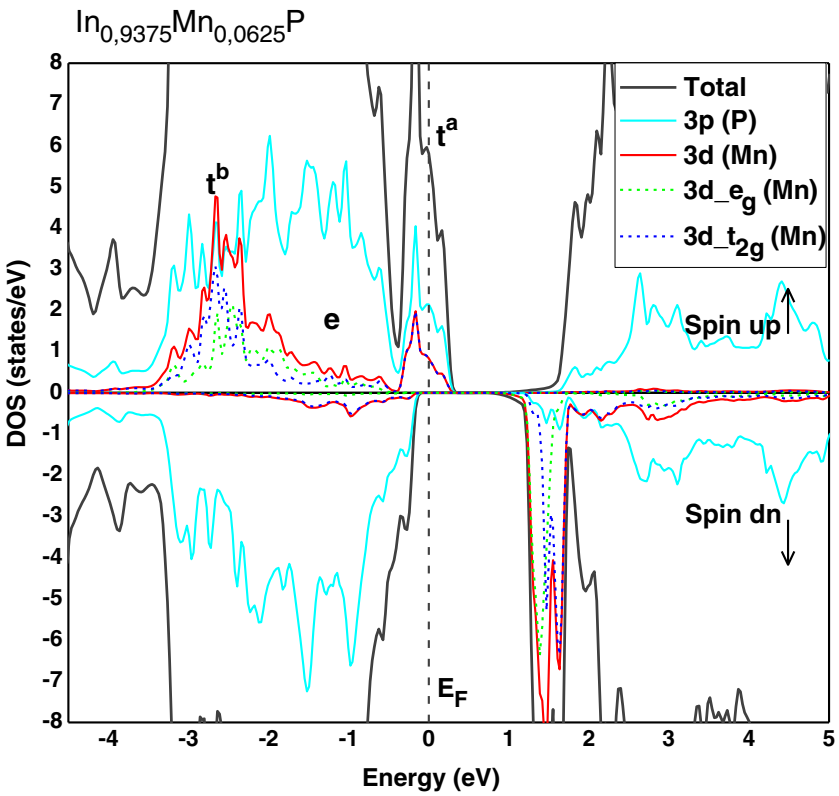

Fig. 5 Spin-polarized total and partial DOS of (3*p*) of P and (3*d*, 3*d*-e_g, 3*d*-t_{2g}) of Mn in supercell for $In_{0.9375}Mn_{0.0625}P$. The Fermi level is set to zero (*dotted line*)

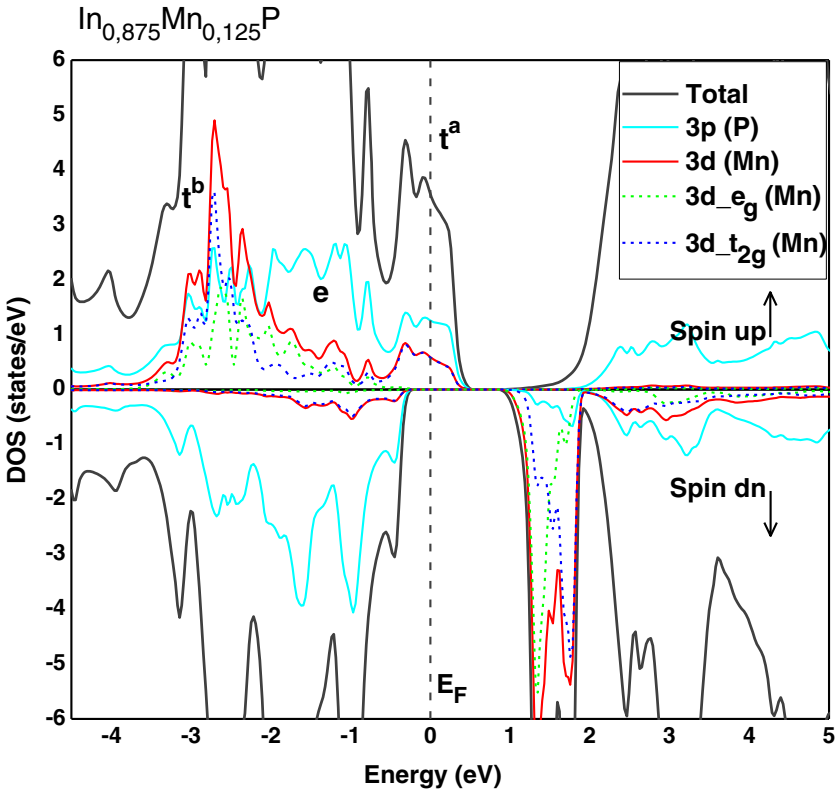

Fig. 6 Spin-polarized total and partial DOS of (3*p*) of P and (3*d*, 3*d*-e_g, 3*d*-t_{2g}) of Mn in supercell for $In_{0.875}Mn_{0.125}P$. The Fermi level is set to zero (*dotted line*)

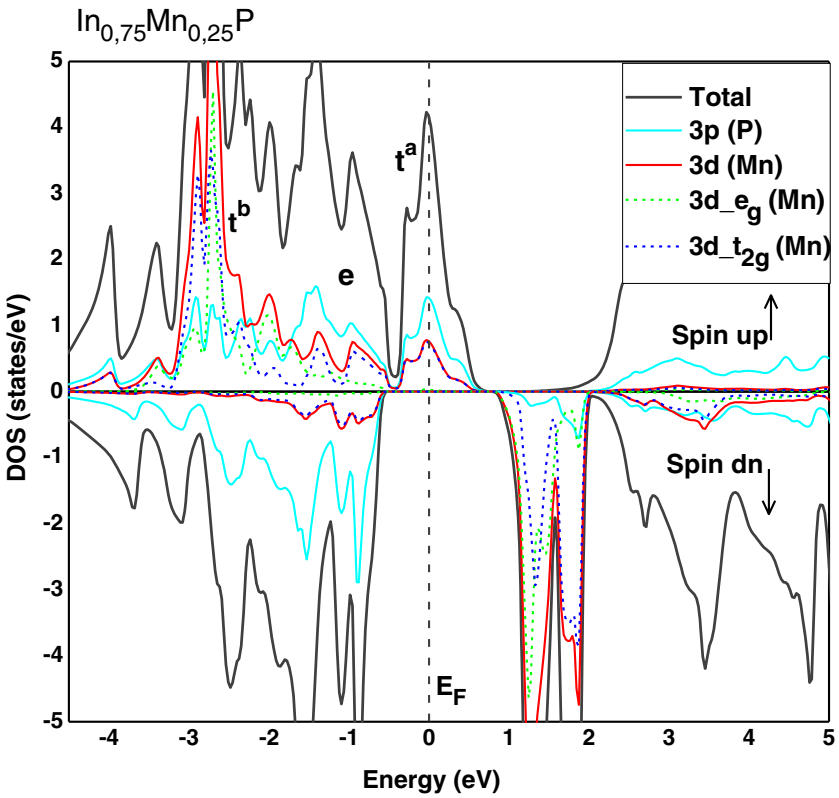

Fig. 7 Spin-polarized total and partial DOS of (3*p*) of P and (3*d*, 3*d*-e_g, 3*d*-t_{2g}) of Mn in supercell for $In_{0.75}Mn_{0.25}P$. The Fermi level is set to zero (*dotted line*)

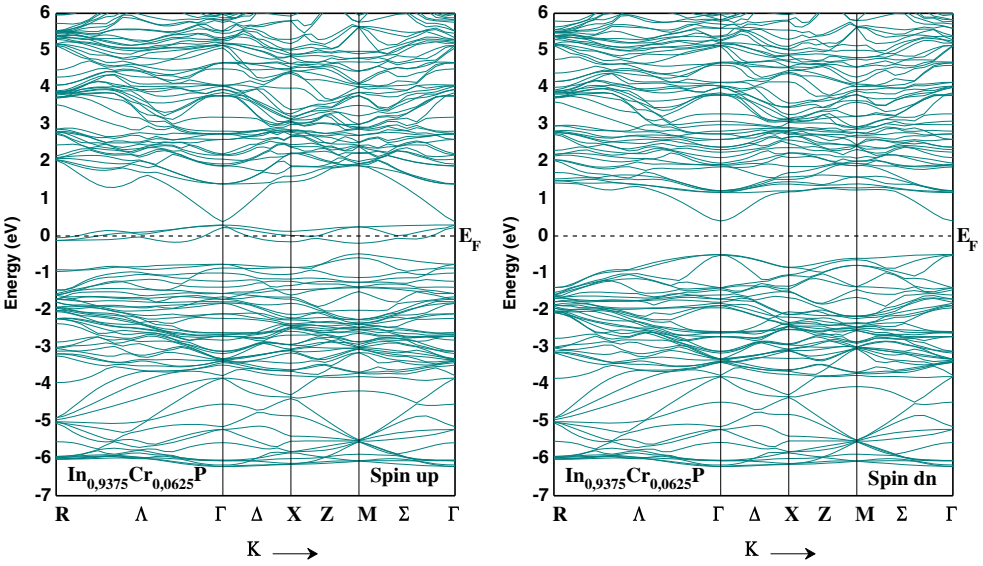

Fig. 8 Spin-polarized band structures for majority spin (*up*) and minority spin (*dn*) for $In_{0.9375}Cr_{0.0625}P$. The Fermi level is set to zero (*dotted line*)

characterized by the *p–d* hybridization that crosses the Fermi level, which leads to 100 % spin polarization. However, in the $In_{1-x}TM_xP$ compounds, the (TM = Cr, Mn) atom substituted at the cationic In site and contributes three electrons for bonding (t^b) states formed by 3*p* (P) states. Consequently, the valence electron configurations of (TM = Cr, Mn) in $In_{1-x}TM_xP$ are Cr^{+3} (d^3-e_g^2 t_{2g}^1) and Mn^{+3} (d^4-e_g^2 t_{2g}^2). Therefore, the 3*d* (TM) minority-spin states are unoccupied, whereas the 3*d* (TM) majority-spin states are not filled, because e_g (Cr, Mn) states are completely filled by two electrons, while the t_{2g} states are partially filled with one electron for Cr and two electrons for Mn. Thus, according to Hund's rule, the valence of partially filled majority-spin states are three electrons for 3*d* (Cr) and four electrons for 3*d* (Mn), which provides a total magnetic moment of $3\mu_B$ and $4\mu_B$ (μ_B is the Bohr magneton), respectively.

Moreover, Sato et al. [47, 50, 51] explain the magnetism of DMS by a simple rule; the ferromagnetic state is stable by the double-exchange mechanism when the delocalized anti-bonding (t^a) states are partially occupied. However, the *p–d* hybridization between 3*p* (P) and 3*d*-t_{2g} (TM = Cr, Mn) majority-spin states exhibits a metallic character in $In_{1-x}TM_xP$ at all concentrations, and this forms the delocalized anti-bonding (t^a) states in the gap. It can be concluded that the anti-bonding nature of partially filled 3*d*-t_{2g} (TM = Cr, Mn) majority-spin states lowers the total energy to stabilize a ferromagnetic ground-state configuration associated with the double-exchange mechanism [52]. Based on our further predictions, we suggest that both

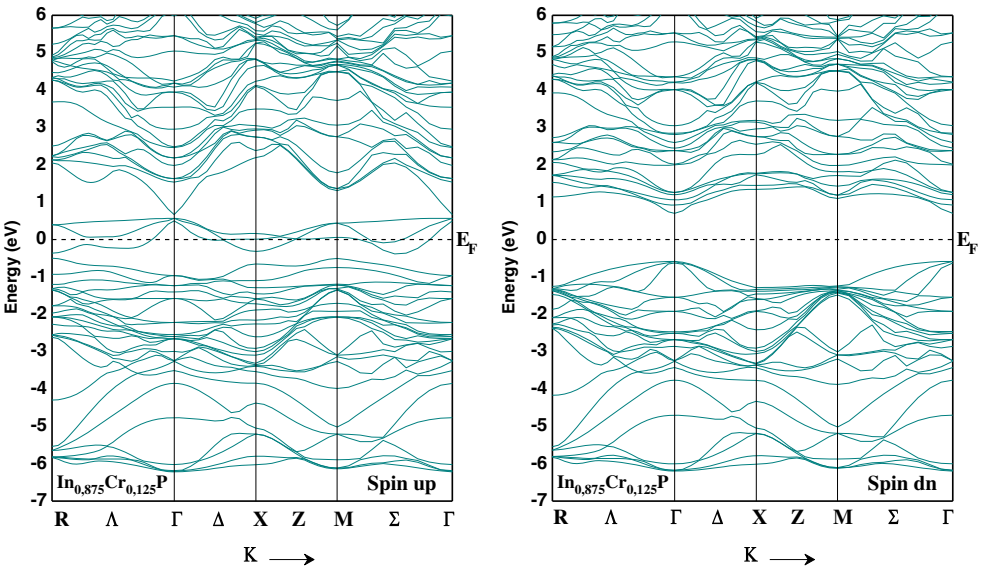

Fig. 9 Spin-polarized band structures for majority spin (*up*) and minority spin (*dn*) for $In_{0.875}Cr_{0.125}P$. The Fermi level is set to zero (*dotted line*)

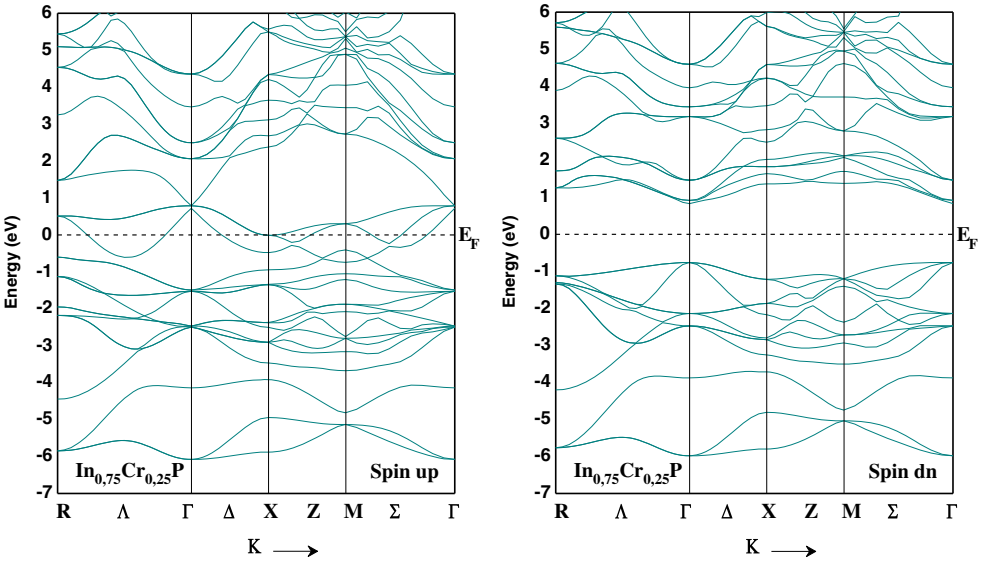

Fig. 10 Spin-polarized band structures for majority spin (*up*) and minority spin (*dn*) for $In_{0.75}Cr_{0.25}P$. The Fermi level is set to zero (*dotted line*)

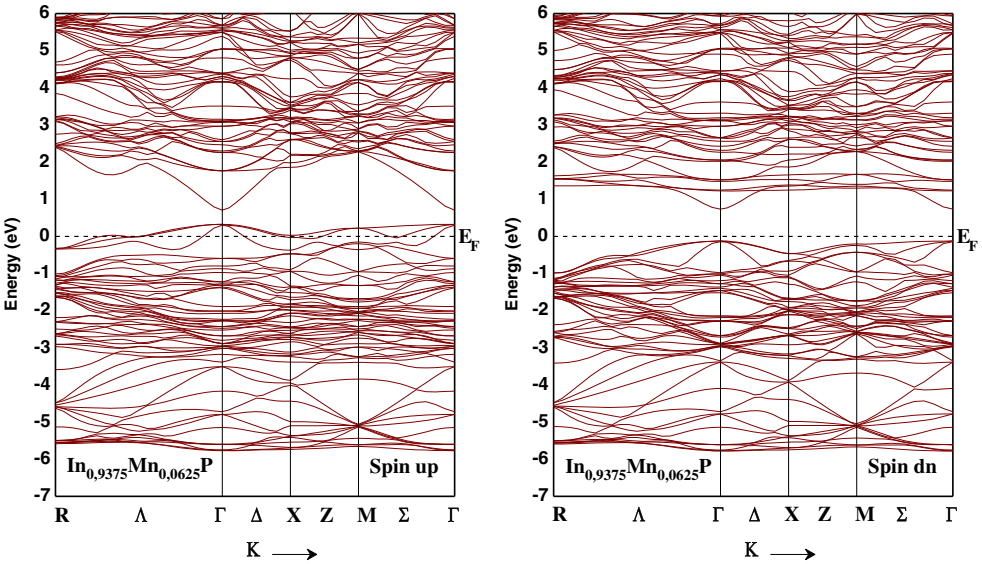

Fig. 11 Spin-polarized band structures for majority spin (*up*) and minority spin (*dn*) for $In_{0.9375}Mn_{0.0625}P$. The Fermi level is set to zero (*dotted line*)

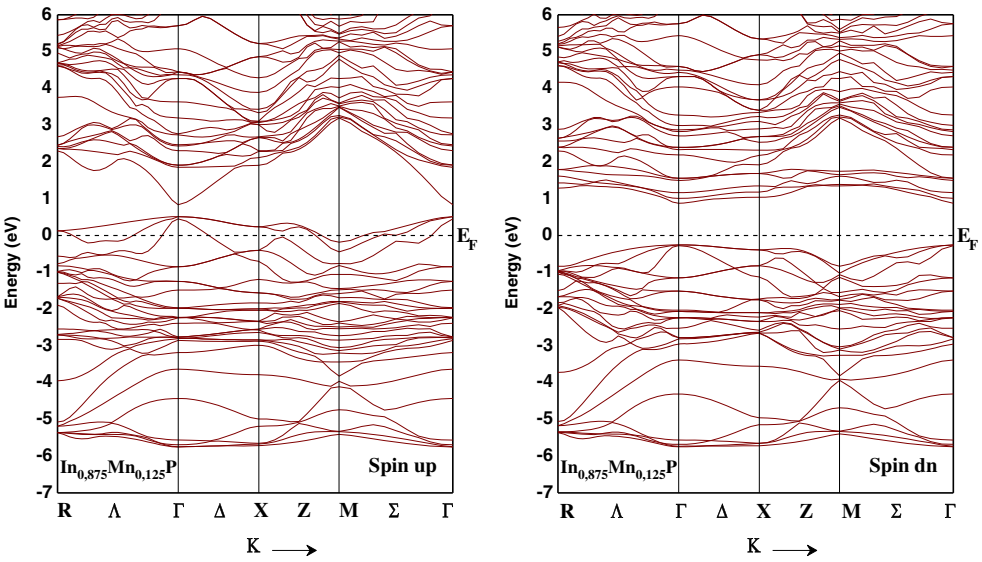

Fig. 12 Spin-polarized band structures for majority spin (*up*) and minority spin (*dn*) for $In_{0.875}Mn_{0.125}P$. The Fermi level is set to zero (*dotted line*)

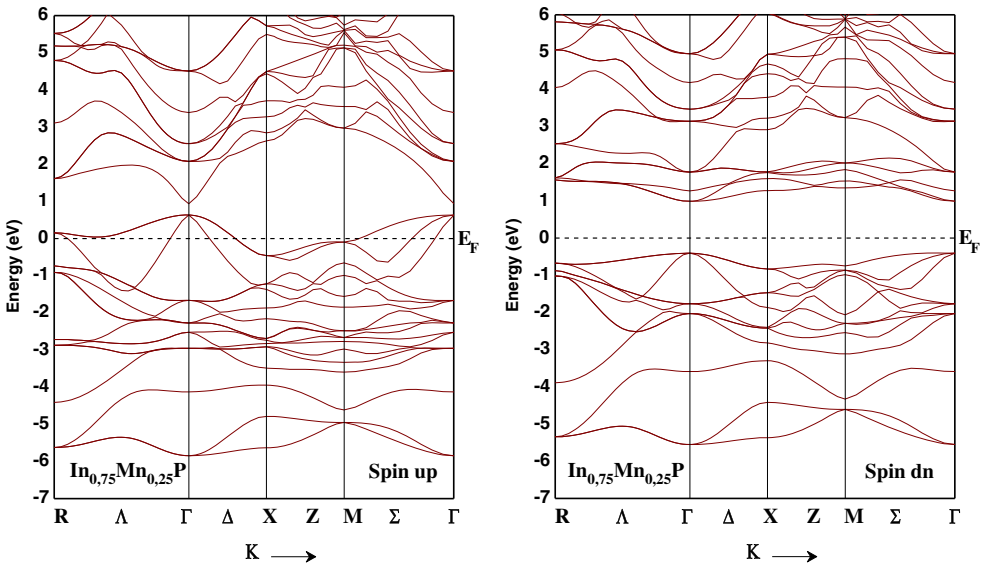

Fig. 13 Spin-polarized band structures for majority spin (*up*) and minority spin (*dn*) for $In_{0.75}Mn_{0.25}P$. The Fermi level is set to zero (*dotted line*)

double-exchange and *p–d* exchange mechanisms contribute to the stabilization of ferromagnetic ground-state configuration in $In_{1-x}TM_xP$ compounds. This suggestion is analogous to the one proposed in the case of $(Al, Ga)_{1-x}Mn_xN$ at concentrations ($x = 0.0625, 0.125, 0.25$) [6].

The calculated spin-dependent band structures along high-symmetry directions in the first Brillouin zone for $In_{0.9375}Cr_{0.0625}P$,$In_{0.875}Cr_{0.125}P$, $In_{0.75}Cr_{0.25}P$, $In_{0.9375}Mn_{0.0625}P$, $In_{0.875}Mn_{0.125}P$, and $In_{0.75}Mn_{0.25}P$ are presented by Figs. 8, 9, 10, 11, 12, and 13, respectively. One can notice that the band structures of $In_{1-x}TM_xP$ (TM = Cr, Mn) show a half-metallic behavior with the majority-spin bands being metallic and the minority-spin bands being semiconducting. The majority-spin bands are more in number than the minority-spin bands due to *p–d* exchange interaction. This provides a half-metallic (HM) gap in minority-spin states, which is an important parameter to determine the application in spintronic devices. However, the HM gap is determined as the minimum between the lowest energy of majority-spin and (minority-spin) conduction bands with respect to the Fermi level and the absolute values of the highest energy of majority-spin and (minority-spin) valence bands [53, 54].

Furthermore, the computed half-metallic ferromagnetic band gap E_g (eV) and HM gap G_h (eV) of minority-spin directions of $In_{1-x}Cr_xP$ and $In_{1-x}Mn_xP$ as a function of the concentration (x) are listed in Table 2. It is observed in band structures that the band gaps (E_g) are located at the Γ point of the Brillouin zone, indicating that the minority-spin channels have a direct band gap for $In_{1-x}Cr_xP$ and $In_{1-x}Mn_xP$ at all concentrations. The energy gap (E_g) increases with increasing concentration (x) of (TM = Cr, Mn) and decreases from $In_{1-x}Cr_xP$ to $In_{1-x}Mn_xP$ at any concentration x. Also, for the minority-spin bands, the maximum of valence band moves towards the Fermi level with decreasing of concentration x. Hence, the HM gap increases from $In_{1-x}Mn_xP$ to $In_{1-x}Cr_xP$, when increasing the concentrations of (TM = Cr, Mn) doping systems. It is found that the impurity bands broaden more strongly. We can notice that the HM gap at a low concentration $x = 0.0625$ for $In_{0.9375}Cr_{0.0625}P$ is 0.404 eV that is larger than 0.125 eV for $In_{0.9375}Mn_{0.0625}P$, which indicates that Cr-doped InP seems to be a more potential candidate than the Mn-doped InP for spin injection applications in the field of spintronic devices.

3.3 Magnetic Properties

The calculated total and local magnetic moment within the muffin–tin spheres of the relevant TM, In, and P atoms and in the interstitial sites of $In_{1-x}TM_xP$ as a function of (TM = Cr, Mn) concentration is shown in Table 3. Due to the *p–d* interaction between 3*d* (TM = Cr, Mn) and 3*p* (P) states, the top of the valence bands are partially filled in

Table 2 Calculated half-metallic ferromagnetic band gap E_g and half-metallic gap G_h of minority spin for $In_{1-x}Cr_xP$ and $In_{1-x}Mn_xP$ at concentrations ($x = 0.0625, 0.125, 0.25$)

Compound	Concentration (x)	E_g (eV)	G_h (eV)
This work			
$In_{1-x}Cr_xP$	0.0625	0.903	0.404
	0.125	1.286	0.586
	0.25	1.595	0.764
$In_{1-x}Mn_xP$	0.0625	0.860	0.125
	0.125	1.130	0.256
	0.25	1.394	0.407

Table 3 Calculated total and local magnetic moment (in Bohr magneton (μ_B)); within the muffin–tin spheres and in the interstitial sites for $In_{1-x}Cr_xP$ and $In_{1-x}Mn_xP$ at concentrations ($x = 0.0625$, 0.125, 0.25)

Compound	Concentration (x)	Total (μ_B)	(Cr, Mn) (μ_B)	In (μ_B)	(P)(μ_B)	Interstitial (μ_B)
This work						
$In_{1-x}Cr_xP$	0.0625	3	2.948	0.044	−0.255	0.267
	0.125	3	2.951	0.034	−0.294	0.321
	0.25	3	2.967	0.026	−0.308	0.318
$In_{1-x}Mn_xP$	0.0625	4	3.854	0.053	−0.187	0.281
	0.125	4	3.863	0.047	−0.198	0.292
	0.25	4	3.978	0.048	−0.269	0.243
Other calculations						
$In_{1-x}Mn_xP$	0.25	4 [8]	3.891 [8]	0.011 [8]	−0.064 [8]	0.212 [8]

majority-spin states, whereas there are empty minority-spin states. It means that the difference in distribution between the two spin channels contributes to ferromagnetism in these materials. It can be understood that the ferromagnetism is induced in $In_{1-x}TM_xP$ by the exchange splitting of the 3*d* bands of the magnetic (TM = Cr, Mn) atoms. Hence, the strong hybridization between 3*d* (TM = Mn, Cr) and 3*p* (P) states provides main magnetic moments in $In_{1-x}TM_xP$ compounds and induces finite magnetization on In atoms as well as the neighboring P atoms and in interstitial sites.

The electronic configurations of TM atoms in $In_{1-x}TM_xP$ show that the 3*d* (TM = Cr, Mn) majority spin states are partially filled by three electrons for Cr and four electrons for Mn impurity. This provides total magnetic moments of $3\mu_B$ for $In_{1-x}Cr_xP$ and $4\mu_B$ for $In_{1-x}Mn_xP$, in which the integer Bohr magneton for a total magnetic moment is a typical characteristic of half-metallic ferromagnets. In addition, the major contributions of total magnetic moments come from the (TM = Cr, Mn) atoms, which are smaller than the predicted values of Hund's rule due to *p–d* hybridization. Moreover, the values of local magnetic moments of (TM = Cr, Mn) increase with an increasing concentration *x* of (TM = Cr, Mn) can be seen in Table 3. However, the negative sign of the local magnetic moment of P atom in $In_{1-x}TM_xP$ shows that the induced magnetic polarization at the P site is anti-parallel to (TM = Cr, Mn) spins, indicating that the interaction between the host valence band carriers and (TM = Cr, Mn) spins is anti-ferromagnetic. Also, the parallel magnetic polarization is initiated at the In site.

Finally, we would like to point out that the spin-polarized band structures can be used to calculate two important parameters. The *s–d* exchange constant $N_0\alpha$ (conduction band) (CB) and the *p–d* exchange constant $N_0\beta$ (valence band) (VB) are exchange constants that can be determined directly from the following mean-field theory expressions [55, 56]:

$$N_0\alpha = \frac{\Delta E_c}{x\,\langle s\rangle}$$

$$N_0\beta = \frac{\Delta E_v}{x\,\langle s\rangle}$$

where $\Delta E_c = E_c^{\downarrow} - E_c^{\uparrow}$ is the conduction band-edge spin-splitting, $\Delta E_v = E_v^{\downarrow} - E_v^{\uparrow}$ is the valence band-edge spin-splitting at the Γ symmetry point, *x* is the concentration of (TM = Cr, Mn), and $\langle s\rangle$ is the half of the computed magnetization per (TM = Cr, Mn) ion [56]. Our calculated values of ΔE_c, ΔE_v, $N_0\alpha$, and $N_0\beta$ are listed in Table 4,

Table 4 Calculated conduction and valence band-edge spin-splitting ΔE_c and ΔE_v and exchange constants $N_0\alpha$ and $N_0\beta$ for $In_{1-x}Cr_xP$ and $In_{1-x}Mn_xP$ at concentrations ($x = 0.0625$, 0.125, 0.25)

Compound	Concentration (x)	ΔE_c (eV)	ΔE_v (eV)	$N_0\alpha$	$N_0\beta$
This work					
$In_{1-x}Cr_xP$	0.0625	0.022	−0.794	0.234	−8.469
	0.125	0.034	−1.151	0.181	−6.138
	0.25	0.041	−1.477	0.109	−3.938
$In_{1-x}Mn_xP$	0.0625	0.029	−0.450	0.232	−3.600
	0.125	0.037	−0.768	0.148	−3.072
	0.25	0.052	−1.038	0.104	−2.076
Other calculations					
$In_{1-x}Mn_xP$	0.025	0.181 [8]	−1.277 [8]	0.362 [8]	−2.554 [8]

and they depict that $N_0\alpha$ decrease and $N_0\beta$ increase as the concentration of (TM = Cr, Mn) increases in $In_{1-x}TM_xP$. We notice that the exchange constant $N_0\beta$ is negative, while the $N_0\alpha$ is positive for $In_{1-x}TM_xP$ at all concentrations ($x =$ 0.0625, 0.125, 0.25) of (TM = Cr, Mn). This indicates that the exchange coupling between VB and 3*d* (TM = Cr, Mn) is anti-ferromagnetic, but it is ferromagnetic between CB and 3*d* (TM = Cr, Mn). This means that the $In_{1-x}Cr_xP$ and $In_{1-x}Mn_xP$ materials exhibit ferromagnetic features.

4 Conclusion

The first-principle calculations of the DFT within the FP-LAPW method and WC-GGA approximation was used to investigate the structural, electronic, and half-metallic ferromagnetic properties in zinc blende phase of $In_{1-x}TM_xP$ (TM = Cr, Mn) at various concentrations ($x = 0.0625$, 0.125, 0.25). We reached the following conclusions:

- The large hybridization between 3*p* (P) and partially filled 3*d* (TM = Cr, Mn) states creates the anti-bonding states in the gap of majority-spin channel, and this stabilizes the ferromagnetic ground state associated with double-exchange mechanism.
- The strong *p*–*d* hybridization reduces the total magnetization of $In_{1-x}Cr_xP$ and $In_{1-x}Mn_xP$ to less than $3\mu_B$ and $4\mu_B$, respectively, and induces smaller contributions on the non-magnetic In and P sites. Thus, the integral value of total magnetization confirms the half-metallic behavior of $In_{1-x}TM_xP$ compounds.
- The $In_{1-x}TM_xP$ (TM = Cr, Mn) at concentrations ($x = 0.0625$, 0.125, 0.25) are half-metallic ferromagnets with half-metallic gaps and 100 % magnetic spin polarization.
- The largest half-metallic gap in $In_{1-x}Cr_xP$ at a low concentration of $x = 0.0625$ reveals that Cr-doped InP seems to be a more potential candidate than the Mn-doped InP for spin injection applications in the field of spintronic devices.

References

1. Prinz, G.A.: J. Magn. Magn. Mater. **200**, 57 (1999)
2. Liu, C., Yun, F., Morkoc, H.: J. Mater. Sci: Mater. Electron. **16**, 555 (2005)
3. Wolf, S.A., et al.: Science **294**, 1488 (2001)
4. Pickett, W.E., Moodera, J.S.: Phys. Today **54**, 39 (2001)
5. Zutic, I., Fabian, J., Das Sarma, S.: Rev. Mod. Phys. **76**, 323 (2004)
6. Doumi, B., Tadjer, A., Dahmane, F., Mesri, D., Aourag, H.: J. Supercond. Nov. Magn. **26**, 515 (2013)
7. Sharma, V., Manchanda, P., Sahota, P.K., Skomski, R., Kashyap, A.: J. Magn. Magn. Mater. **324**, 786 (2012)
8. Djedid, A., Doumi, B., Méçabih, S., Abbar, B.: J. Mater. Sci. **48**, 6074 (2013)
9. Saini, H.S., Singh, M., Reshak, A.H., Kashyap, M.K.: J. Alloy. Compd. **536**, 214 (2012)
10. Ahmad, I., Amin, B.: Comput. Mater. Sci. **68**, 55 (2013)
11. Yao, G., Fan, G., Xing, H., Zheng, S., Ma, J., Zhang, Y., He, L.: J. Mater. Sci. **331**, 117 (2013)
12. Yao, G., Fan, G., Zheng, S., Ma, J., Chen, J., Zhou, D., Li, S., Zhang, Y., Su, S.: Opt. Mater. **34**, 1593 (2012)
13. Dahmane, F., Tadjer, A., Doumi, B., Mesri, D., Aourag, H.: J. Supercond. Nov. Magn. **26**, 3339 (2013)
14. Boukra, A., Zaoui, A., Ferhat, M.: Superlattice. Microstruct. **52**, 880 (2012)
15. Saini, H.S., Singh, M., Reshak, A.H., Kashyap, M.K.: J. Magn. Magn. Mater. **331**, 1 (2013)
16. Sajjad, M., Zhang, H.X., Noor, N.A., Alay-e-Abbas, S.M., Shaukat, A., Mahmood, Q.: J. Magn. Magn. Mater. **343**, 177 (2013)
17. Bourouis, Ch., Meddour, A.: J. Magn. Magn. Mater. **324**, 1040 (2012)
18. Ahmadian, F., Makaremi, N.: Solid State Commun. **152**, 1660 (2012)
19. Huang, Y., Jie, W., Zha, G.: J. Alloy. Compd. **539**, 271 (2012)
20. Huang, Y., Jie, W., Zha, G.: J. Alloy. Compd. **555**, 117 (2013)
21. Li, J., Xu, X., Zhou, Y., Zhang, M., Luo, X.: J. Alloy. Compd. **575**, 190 (2013)
22. Noor, N.A., Alay-e-Abbas, S.M., Saeed, Y., Ghulam Abbas, S.M., Shaukat, A.: J. Magn. Magn. Mater. **339**, 11 (2013)
23. Alay-e-Abbas, S.M., Wong, K.M., Noor, N.A., Shaukat, A., Lei, Y.: Solid State Sci. **14**, 1525 (2012)
24. Doumi, B., Tadjer, A., Dahmane, F., Djedid, A., Yakoubi, A., Barkat, Y., Ould Kada, M., Sayede, A., Hamada, L.: J. Supercond. Nov. Magn. **27**, 293 (2014)
25. Gorodynskyy, V., Zdansky, K., Pekarek, L., Malina, V., Vackova, S.: Nucl. Instr. Meth. A **555**, 288 (2005)
26. Werking, J.D., Bolognesi, C.R., Chang, L.-D., Nguyen, C., Hu, E.L., Kroemer, H.: IEEE Electron. Dev. Lett. **13**, 164 (1992)
27. Soderstrom, J.R., Chow, D.H., McGill, T.C.: Appl. Phys. Lett. **55**, 1094 (1989)
28. Dietl, T., Ohno, H., Matsukura, F., Cibert, J., Ferrand, D.: Science **287**, 1019 (2000)
29. Hollingsworth, J., Bandaru, P.R.: Mater. Sci. Eng. B **151**, 152 (2008)
30. Korona, K.P., Wysmolek, A., Kamińska, M., Twardowski, A., Piersa, M., Palczewska, M., Strzelecka, G., Hruban, A., Kuhl, J., Adomavicius, R., Krotkus, A.: Physica B **382**, 220 (2006)
31. Tarhan, E., Miotkowski, I., Rodriguez, S., Ramdas, A.K.: Phys. Rev. B **67**, 195202 (2003)
32. Schmidt, T.M., Venezuela, P., Arantes, J.T., Fazzio, A.: Phys. Rev. B **73**, 235330 (2006)
33. Hohenberg, P., Kohn, W.: Phys. Rev. B **136**, 864 (1964)
34. Kohn, W., Sham, L.J.: Phys. Rev. A **140**, 1133 (1965)
35. Blaha, P., Schwarz, K., Madsen, G.K.H., Kvasnicka, D., Luitz, J.: WIEN2k, an Augmented Plane Wave Plus Local Orbitals Program for Calculating Crystal Properties. Vienna University of Technology, Vienna (2001)
36. Wu, Z., Cohen, R.E.: Phys. Rev. B **73**, 235116 (2006)
37. Monkhorst, H.J., Pack, J.D.: Phys. Rev. B **13**, 5188 (1976)
38. Pack, J.D., Monkhorst, H.J.: Phys. Rev. B **16**, 1748 (1977)
39. Muranghan, F.D.: Proc. Natl. Acad. Sci. USA **30**, 244 (1944)
40. Tran, F., Laskowski, R., Blaha, P., Schwarz, K.: Phys. Rev. B **75**, 115131 (2007)
41. Heyd, J., Peralta, J.E., Scuseria, G.E., Martin, R.L.: J. Chem. Phys. **123**, 174101 (2005)
42. Wang, S.Q., Ye, H.Q.: Phys. Rev. B **66**, 235111 (2002)

43. Perdew, J.P., Burke, K., Ernzerhof, M.: Phys. Rev. Lett. **77**, 3865 (1996)
44. Zunger, A.: Solid State Phys. **39**, 275 (1986)
45. Cui, X.Y., Delley, B., Freeman, A.J., Stampfl, C.: Phys. Rev. Lett. **97**, 016402 (2006)
46. Singh, R.: J. Magn. Magn. Mater. **322**, 290 (2010)
47. Sato, K., Dederichs, P.H., Araki, K., Katayama-Yoshida, H.: Phys. Status Solidi C **7**, 2855 (2003)
48. Katayama-Yoshida, H., Sato, K.: J. Phys. Chem. Solids **64**, 1447 (2003)
49. Sato, K., Fukushima, T., Toyoda, M., Kizaki, H., Dinh, V.A., Fujii, H., Bergqvist, L., Dederichs, P.H., Katayama-Yoshida, H.: Physica B **404**, 5237 (2009)
50. Sato, K., Katayama-Yoshida, H.: Jpn. J. Appl. Phys. **40**, L485 (2001)
51. Sato, K., Katayama-Yoshida, H., Dederichs, P.H.: J. Supercond. **16**(1), 31 (2003)
52. Akai, H.: Phys. Rev. Lett. **81**, 3002 (1998)
53. Yao, K.L., Gao, G.Y., Liu, Z.L., Zhu, L.: Solid State Commun. **133**, 301 (2005)
54. Gao, G.Y., Yao, K.L., Şaşıoğlu, E., Sandratskii, L.M., Liu, Z.L., Jiang, J.L.: Phys. Rev. B **75**, 174442 (2007)
55. Raebiger, H., Ayuela, A., Nieminen, R.M.: J. Phys. Condens. Matter. **16**, L457 (2004)
56. Sanvito, S., Ordejon, P., Hill, N.A.: Phys. Rev. B **63**, 165206 (2001)